ACS APPLIED MATERIALS & INTERFACES

Letter

www.acsami.org

Deep Level Transient Spectroscopy (DLTS) on Colloidal-Synthesized Nanocrystal Solids

Deniz Bozyigit, Michael Jakob, Olesya Yarema, and Vanessa Wood*

Laboratory for Nanoelectronics, Department of Information Technology and Electrical Engineering, Eidgenoessische Technische Hochschule Zurich

Supporting Information

ABSTRACT: We demonstrate current-based, deep level transient spectroscopy (DLTS) on semiconductor nanocrystal solids to obtain quantitative information on deep-lying trap states, which play an important role in the electronic transport properties of these novel solids and impact optoelectronic device performance. Here, we apply this purely electrical measurement to an ethanedithiol-treated, PbS nanocrystal solid and find a deep trap with an activation energy of 0.40 eV and a density of $N_T = 1.7 \times 10^{17}$ cm^{-3}. We use these findings to draw and interpret band structure models to gain insight into charge transport in PbS nanocrystal solids and the operation of PbS nanocrystal-based solar cells.

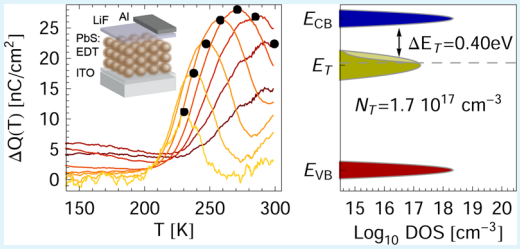

KEYWORDS: *semiconductor nanocrystals, PbS, nanocrystal solid, DLTS, charge trapping, solar cells, Schottky interface*

INTRODUCTION

New semiconductor materials, manufactured using low-cost, solution-based processes, have rapidly gained interest for next generation electronic and optoelectronic devices. For example, solids of colloidally synthesized semiconductor nanocrystals (NCs) are explored for field-effect transistors (FETs),[1,2] LEDs,[3] and photovoltaics (PVs),[4−8] although performance must be improved prior to commercialization. For conventional solar cells, it is known that the presence of trap states acting as recombination centers strongly limits their performance and it is believed that such trap states currently limit the performance of NC-based devices. First demonstrations of chemical treatments on PbS NC solids have shown improved PV performance, which is believed to result from the passivation of trap states.[2,9,10] To confirm this hypothesis and further improve chemical treatment strategies, it is necessary to be able to reliably quantify the density and properties of trap states in NC solids. This has led to a growing interest in techniques to characterize trap states and their impact on charge transport.[9−13]

In this work, we demonstrate for the first time that deep level transient spectroscopy (DLTS) can be used to quantify the density of traps (N_T), the trap energy (E_T), and the capture cross-section (σ_T) of traps in NC solids. All DLTS methods are based on measurement of a transient signal (voltage, capacitance, current, or charge) over a range of temperatures to extract the properties of charge traps (N_T, ΔE_T, σ_T). In the initial demonstrations of DLTS on conventional semiconductors, capacitance transients were measured,[14] where the space charge region (SCR) acts as a transducer between the charge in the traps and the measured SCR-capacitance. This requires a detailed understanding of the SCR and large trap densities are known to invalidate the underlying assumptions of capacitance-based DLTS.[15] This may be the reason why earlier attempts at DLTS on CdSe NCs on a TiO_2 electrode did not yield conclusive results.[16] We instead utilize a current-based DLTS method[17] (often referred to as Q-DLTS), which employs the measurement of current transients and was particularly successful for organic materials.[18,19]

As an initial system to study, we select a solid of PbS NCs with an ethanedithiol (EDT) surface treatment since it is commonly used as the active material in a variety of NC solar cells, and the performance limitations are believed to be linked to the presence of trap states.[4−8,10] We apply our findings on PbS NC solids to elucidate the picture of band structure and charge transport in this novel semiconductor.

EXPERIMENT AND RESULTS

A solid formed from a PbS NC-solution is incorporated into a Schottky diode-type solar cell as described in the Supporting Information (Figure 1a, b). Figure 1c, d shows the current density versus voltage characteristics of the device in the dark (black) and under AM1.5G illumination (red). We observe a typical diode with a rectification of >100 and a small hysteresis. We determine an open-circuit voltage (V_{oc}) of 0.47 V, a short-circuit current (J_{sc}) of 9.7 mA/cm^2, a fill-factor of 51%, and a power conversion efficiency of 2.3%, comparable to literature values.[7,20]

We perform the current-based DLTS measurements using the experimental setup depicted in Figure 2a. We apply a reverse bias (V_D = −0.7 V) to the device and a 1 ms voltage pulse every 10 ms (see Figure 2c), while simultaneously

Received: January 24, 2013
Accepted: March 25, 2013
Published: March 25, 2013

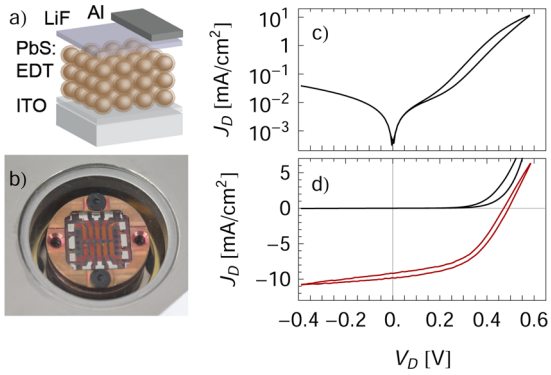

Figure 1. (a) Schematic of the Schottky junction solar cell. (b) Photograph of device in cryostat. (c, d) Current–density versus voltage for the solar cell examined in the dark (black line) and under AM1.5G illumination (red line). The device shows a clear diode behavior with a rectification >100 and a small hysteresis and a power conversion efficiency of 2.3%, typical of literature values.

measuring the current density through the device ($J_D(t)$). During the forward section of the pulse (V_D = 0 V), traps in the SCR can be populated (Figure 2b, top). At time t = 0, when the reverse bias is again applied, the populated traps can emit the captured charge carriers so as to thermalize to the new bias condition. This carrier emission process is observed as a current transient in the device current signal (Figure 2d). For sample temperatures of 131–299 K, we obtain the trap emission current $J_E(t)$ (Figure 2e) by removing the influence of the capacitive displacement current (J_{cap}) and the reverse leakage current (J_{leak}) as described in the Supporting Information. In the raw transient data in Figure 2e, we observe that at least two temperature-dependent time constants govern the decay process. We will explain in the following how these transient can be used to extract information on trap states.

Based on the Shockley–Read–Hall (SRH) model, the current originating from emitting traps is given by

$$J_E(t) = \sum_i \frac{WN_{T,i}}{\tau_{E,i}} \exp\left(-\frac{t}{\tau_{E,i}}\right) \quad (1)$$

where W is the width of the SCR, $N_{T,i}$ is the volume density, and $\tau_{E,i}$ is the emission time constant for a trap of type i. Assuming that charge carrier emission is a thermally activated process, the emission time constant for each trap type i is given by

$$\tau_{E,i} = \sigma_{T,i}^{-1}\Gamma_{p(n)}^{-1}T^{-2}\exp\left(-\frac{\Delta E_{T,i}}{kT}\right) \quad (2)$$

where $\sigma_{T,i}$ is the cross-section of the trap, $\Delta E_{T,i}$ is the activation energy of the trap to a transporting band, k the Boltzmann constant, and T the temperature of the system. The material-dependent factor $\Gamma_{p(n)}$ is given by

$$\Gamma_{p(n)} = 2 \times 3^{1/2}(2\pi/h^2)^{3/2}k^2 m^*_{p(n)} = 3.256 \times 10^{20}\ \mathrm{K^{-2}\ cm^{-2}\ s^{-1}} \quad (3)$$

where h is the Planck constant and $m^*_{p(n)} = 0.1m_e$ the effective mass of the free holes (and electrons) in bulk PbS.[21] Equation 2 shows that emission time constants become long at low temperatures, such that traps are not (de)populated in the time window of observation (i.e., they freeze out). On the basis of eq

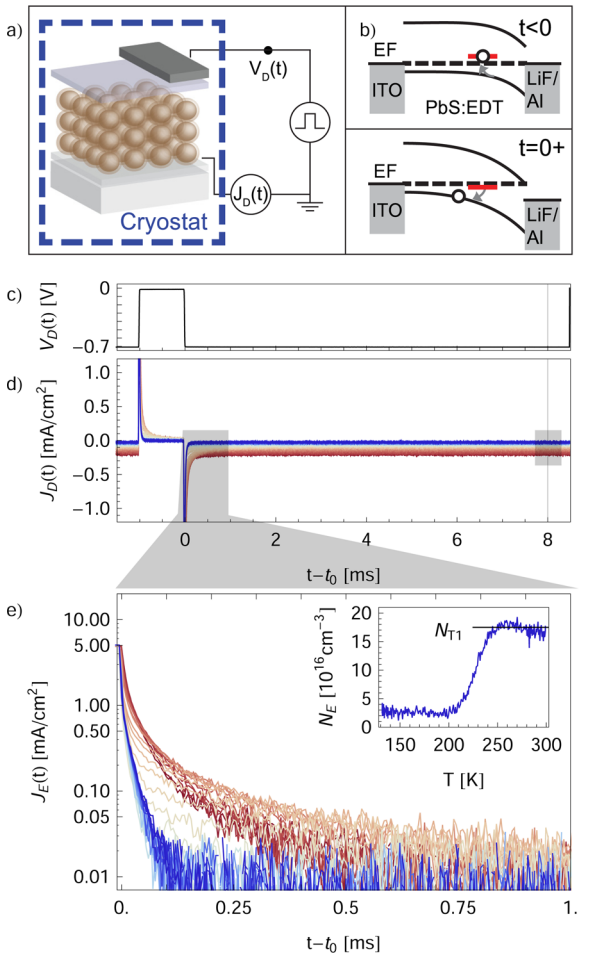

Figure 2. (a) Schematic of the DLTS measurement setup. Voltage pulses (V_D) are applied to the diode while the current density (J_D) is measured. (b) Schematic of the band diagrams before (t < 0) and after (t = 0$^+$) the voltage step. After the step, previously occupied traps adjust to the new bias condition by emitting carriers that can be measured as a current transient. (c) Time trace of the voltage applied to the device (V_D). (d) Measurement of the current through the device (J_D) for temperatures between 131 K (blue) to 300 K (red). The current value at t = 8 ms is used to estimate the leakage current (J_{leak}). The leakage current is always smaller than 2.5 mA/cm^2, demonstrating that no device breakdown occurs during the measurements. (e) Transients of the trap emission current (J_E) show two time constants. With decreasing temperature, the long time constant transient first becomes slower (red to orange) and then disappears (orange to blue). This is the expected behavior for a trap emission current. The inset shows the total density of emitted carriers (N_E) calculated from J_E. Close to room temperature, we find a constant number of emitted carriers, N_{T1} = 1.7 × 10^{17} cm^{-3}.

1, the total density of emitted carriers (N_E) can be determined by integrating the measured J_E

$$N_E = \frac{1}{Wq}\int J_E(t)dt = \sum_i N_{T,i} \quad (4)$$

where q is the electron charge. In Figure (2e inset) we plot N_E versus temperature and can clearly distinguish two regions. At 300 K, a trap density of $N_{T,1}$ = 1.7 × 10^{17} cm^{-3} is measured, which start to freeze out at 250 K. Below 200 K, only a residual charge density of 3 × 10^{16} cm^{-3} is observed.

dx.doi.org/10.1021/am400326t | ACS Appl. Mater. Interfaces 2013, 5, 2915–2919

We can now use the same current transient data to extract the trap activation energy (ΔE_T) and the cross-section (σ_T) by calculating the DLTS spectrum (ΔQ)

$$\Delta Q = Q(t_2) - Q(t_1) = \int_{t_1}^{t_2} J_E(t)dt \quad (5)$$

where t_1 and t_2 are two times that can be freely chosen to define a detector time constant given by $\tau_Q = (t_2 - t_1)/(\log t_2/t_1)$. In Figure 3a, we plot ΔQ vs temperature for a fixed ratio $t_2/t_1 = 5$

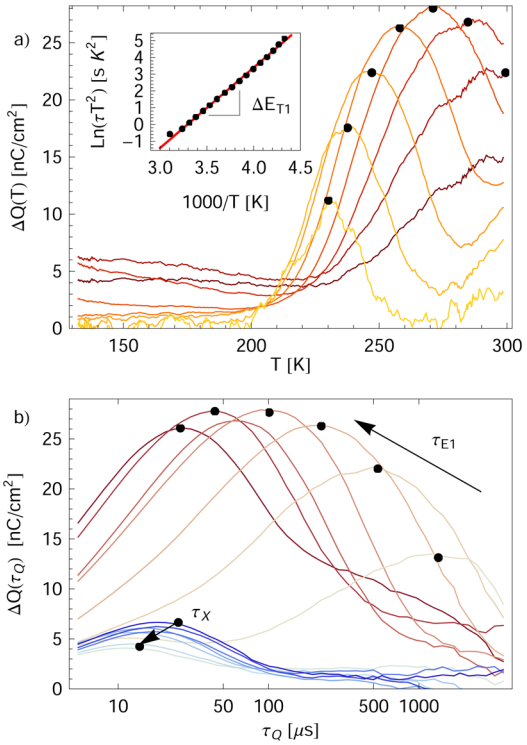

Figure 3. (a) DLTS spectrum (ΔQ) vs temperature (T) for different detector time constants (τ_Q). The Arrhenius plot in the inset relates the temperature at which the peak in ΔQ occurs and the corresponding τ_Q. The linear fit reveals an activation energy of $\Delta E_{T,1}$ = 0.40 eV and a cross-section $\sigma_{T,1} = 1.6 \times 10^{-14}$ cm^2. (b) The same spectrum (ΔQ) as in (a) plotted vs τ_Q for temperatures between 131 K (blue) and 300 K (red). The thermally activated emission time constant (τ_{E1}) is clearly visible. Additionally a weakly temperature dependent time constant $\tau_X \approx 20$ μs is present. This time constant is attributed to transport within the trap band.

and τ_Q between 10 and 1 ms. A peak appears at the temperatures where the trap emission time τ_E equals τ_Q. On the basis of eq 2, we plot the peak temperatures in an Arrhenius-type plot in Figure 3a, inset, and find a linear dependence that allows to extract an activation energy of $\Delta E_{T,1}$ = 0.40 eV from the slope and a capture cross-section $\sigma_{T,1} = 1.6 \times 10^{-14}$ cm^2 from the y-intercept.

Plotting the same data along the τ_Q axis in Figure 3b, we can see the emission time constant τ_{E1} of the trap reducing with increasing temperatures. Furthermore we observe a second peak with a time constant $\tau_X \approx 20$ μs with a weak temperature dependence. Because of this weak temperature dependence, we do not interpret this time constant as an emission time of a second deep trap state; instead, we attribute τ_X to a transport process with a low mobility, which can be estimated to be $d^2/(2\tau_X V_D) = 1.6 \times 10^{-6}$ cm^2/(V s). The total charge density in this process is 3×10^{16} cm^{-3} as determined from Figure 2f .

DISCUSSION

Our DLTS measurements show the presence of (1) an abundant trap state (hereafter, *T1 trap*) with an activation energy of 0.40 eV and density of 1.7×10^{17} cm^{-3} and (2) a weakly temperature dependent, low-mobility (1.6×10^{-6} cm^2/(V s)) transport process (hereafter, *process X*) with a carrier density of of 3×10^{16} cm^{-3}. DLTS does not determine whether carriers in the T1 traps are thermally activated to the valence band (VB) or to the conduction band (CB) and whether the T1 trap is of acceptor or donor type. DLTS does also not indicate in which band transport process X occurs. Therefore, DLTS measurements must be interpreted in the context of a specific band structure picture. In the discussion below, we consider two models: the model of a PbS NC solid as a conventional p-type semiconductor and the model of a PbS NC solid with a metallic midgap band, proposed recently by Nagpal and Klimov.[11] To calculate the band alignment at the PbS/Al interface consistently for both models (Figure 4a, b), we adopt the strong but often used assumption[8,22,23] that the CB and VB in a NC solid stem directly from the lowest quantum confined states that are the source of the photoluminescence (PL) of the

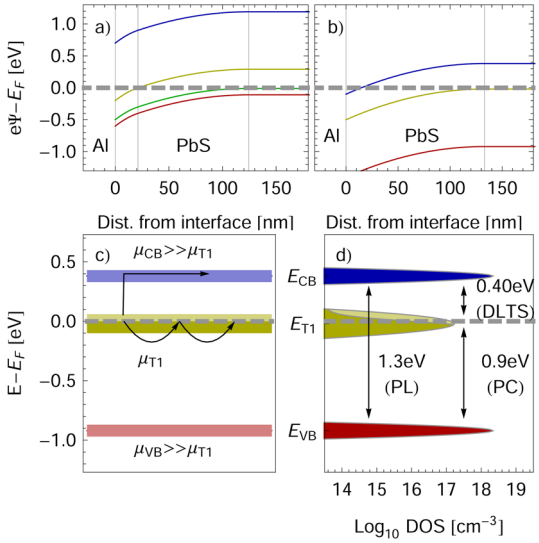

Figure 4. (a) Band diagram for the PbS/Al Schottky junction under the assumptions that the PbS NC solid is a conventional p-type SC (i.e., the Fermi energy (E_F) is close to the VB (red) due to an intrinsic acceptor dopant (green)). In this picture the T1 trap (yellow) has to be of acceptor type and close to the VB. Within the space charge region (SCR), the E_F crosses the T1 energy, which should be detectable by capacitance voltage measurements. (b) Band diagram within the model of Nagpal,[11] where the T1 trap (yellow) forms a metallic midgap band close to the CB (blue). The width and built-in voltage of the SCR are identical to the model considered in (a). (c) Schematic of the two transport processes in PbS NC solid for the model in (b). The VB (red) and the CB (blue) are separated by the optical bandgap of the NCs (1.3 eV). The trap T1 (yellow) is located 0.4 eV below the CB and forms a band. DLTS measurements show emission of carriers from traps by thermal activation into the CB and direct hopping within the T1 band with a low mobility of $\mu_{T1} = 1.6 \times 10^{-6}$ cm^2/(Vs). (d) The density of states of the T1 band is determined by DLTS to be on the order of 1.7×10^{17} cm^{-3} with a small amount of free holes (3×10^{16} cm^{-3}) in the T1 band. Energies are annotated by the technique by which they are determined.

dx.doi.org/10.1021/am400326t | ACS Appl. Mater. Interfaces 2013, 5, 2915−2919

individual NCs. For our PbS NC material, we find $E_{VB}-E_{CB}$ = 1.3 eV from the optical bandgap. Because there is no consensus on the distance of either band to the vacuum level E_{vac}, we further assume a Fermi energy $E_F = E_{vac}-4.7$ eV (see the Supporting Information).

The most popular model for PbS NC solids has been that of a conventional p-type semiconductor where conduction is mediated by holes in the VB.[22,24,25] A carrier density on the order of 3×10^{16} cm^{-3} has been previously extracted from capacitance voltage measurements and, in the context of the model of PbS as a p-type semiconductor, interpreted as intrinsic p-type dopants stemming from oxygen or water related defects.[22] We therefore assume that our observed transport process X is a measurement of hole transport in the valence band and that our T1 traps are of acceptor type and located 0.4 eV above the VB. Using the quantitative values from DLTS for T1 and X, we calculate the resulting PbS/Al junction band diagram by solving Poissons equation (Figure 4a).

We also consider a new model, recently put forward by Nagpal and Klimov based on photocurrent (PC) measurements in PbS NC FET structures,[11] which postulates the existence of a nearly full, metallic midgap band, 0.4 eV below the CB in NCs with a 1.3 eV bandgap, in agreement with earlier reports on photodetectors.[26] Conduction in the dark is related to low-mobility carriers in the midgap band, while photoconduction is mediated by high mobility carriers in the VB or CB. Figure 4c illustrates how we can explain our DLTS measurements in the context of this model by identifying the T1 trap as the midgap band and transport process X as carrier motion within this midgap band. The model of a metallic midgap band implies that carriers can move slowly within the midgap band without thermal activation (Figure (4c)) consistent with the weak temperature dependence of the transport process X. If temperatures are high enough, electrons can be thermally activated from the midgap band into the high mobility CB and are swept out quickly. This process is consistent with the observation of the thermally activated T1 trap in our DLTS measurements. Furthermore, the thermal activation energy (0.4 eV) determined with DLTS is in quantitative agreement with the midgap energy measured optically in ref.[11] We again calculate the expected band alignment at the PbS/Al interface (Figure 4b). The resulting SCR appears nearly identical (width of 125 nm and built-in voltage of 0.5 V) to the SCR predicted using the model of a p-type semiconductor (Figure 4a), even though the band diagram and conduction mechanism are different in the two models. This highlights why simple characterization methods like capacitance voltage or current voltage measurements alone are unlikely to discriminate between models.

However, current-based DLTS provides information on the trap state energies and densities and time scales associated with trapping and transport. The quantitative values obtained with DLTS show us that, in the model of PbS as a p-type semiconductor, the T1 level would cross the Fermi energy within the SCR (Figure 4a). This crossing splits the SCR in two regions, which is a known phenomenon in other materials in the presence of large trap densities and should be detectable by frequency dependent capacitance–voltage measurements.[15,27] In conclusion, although DLTS does not rule out the model of a PbS NCs solid as a p-type semiconductor, the agreement in energy and transport time scales strongly supports the model of a midgap band formed by charge carrier traps. Furthermore, our DLTS measurements suggest a clear experiment to test the model of a p-type semiconductor. Looking forward, the quantitative information that can be obtained from DLTS underscores its potential to aid in the understanding of charge transport in NC solids and the rational selection of chemical treatments and interface preparation to enhance the performance of NC-based devices.

■ ASSOCIATED CONTENT

Supporting Information

A detailed description of nano crystal synthesis, device fabrication, the DLTS measurement setup, investigations on the applicability of capacitance-based DLTS and the calculation of the band diagrams. This material is available free of charge via the Internet at http://pubs.acs.org/.

■ AUTHOR INFORMATION

Corresponding Author

*E-mail: vwood@ethz.ch.

Notes

The authors declare no competing financial interest.

■ ACKNOWLEDGMENTS

The authors thank K. McPeak and the OMEL at ETHZ for helpful discussions. Funding for this project was supported by the Swiss National Science Foundation (SNSF). TEM was performed at the Electron Microscopy ETH Zurich (EMEZ).

■ REFERENCES

(1) Lee, J.-S.; Kovalenko, M. V.; Huang, J.; Chung, D. S.; Talapin, D. V. *Nat. Nanotechnol.* **2011**, *6*, 348–52.
(2) Chung, D. S.; Lee, J.-S.; Huang, J.; Nag, A.; Ithurria, S.; Talapin, D. V. *Nano Lett.* **2012**, *12*, 1813–20.
(3) Kwak, J.; Bae, W. K.; Lee, D.; Park, I.; Lim, J.; Park, M.; Cho, H.; Woo, H.; Yoon, D. Y.; Char, K.; Lee, S.; Lee, C. *Nano Lett.* **2012**, *12*, 2362–6.
(4) Ma, W.; Luther, J. M.; Zheng, H.; Wu, Y.; Alivisatos, A. P. *Nano Lett.* **2009**, *9*, 1699–703.
(5) Luther, J. M.; Gao, J.; Lloyd, M. T.; Semonin, O. E.; Beard, M. C.; Nozik, A. J. *Adv. Mater.* **2010**, *22*, 3704–7.
(6) Zhao, N.; Osedach, T. P.; Chang, L.-Y.; Geyer, S. M.; Wanger, D.; Binda, M. T.; Arango, A. C.; Bawendi, M. G.; Bulovic, V. *ACS Nano* **2010**, *4*, 3743–52.
(7) Szendrei, K.; Gomulya, W.; Yarema, M.; Heiss, W.; Loi, M. A. *Appl. Phys. Lett.* **2010**, *97*, 203501.
(8) Gao, J.; Luther, J. M.; Semonin, O. E.; Ellingson, R. J.; Nozik, A. J.; Beard, M. C. *Nano Lett.* **2011**, *11*, 1002–8.
(9) Tang, J.; Kemp, K. W.; Hoogland, S.; Jeong, K. S.; Liu, H.; Levina, L.; Furukawa, M.; Wang, X.; Debnath, R.; Cha, D.; Chou, K. W.; Fischer, A.; Amassian, A.; Asbury, J. B.; Sargent, E. H. *Nat. Mater.* **2011**, *10*, 765–771.
(10) Ip, A. H.; Thon, S. M.; Hoogland, S.; Voznyy, O.; Zhitomirsky, D.; Debnath, R.; Levina, L.; Rollny, L. R.; Carey, G. H.; Fischer, A. L.; et al. *Nat. Nanotechnol.* **2012**, *7*, 577–582.
(11) Nagpal, P.; Klimov, V. I. *Nat. Commun.* **2011**, *2*, 486.
(12) Szendrei, K.; Speirs, M.; Gomulya, W.; Jarzab, D.; Manca, M.; Mikhnenko, O. V.; Yarema, M.; Kooi, B. J.; Heiss, W.; Loi, M. A. *Adv. Funct. Mater.* **2012**, *22*, 1598–1605.
(13) Gao, J.; Johnson, J. C. *ACS NANO* **2012**, *6*, 3292–303.
(14) Lang, D. V. *J. Appl. Phys.* **1974**, *45*, 3023.
(15) Lang, D. V. *Top. Appl. Phys.* **1979**, *37*, 93–133.
(16) Loef, R.; Houtepen, A. J.; Talgorn, E.; Schoonman, J.; Goossens, A. *J. Phys. Chem. C* **2009**, *113*, 15992–15996.
(17) Borsuk, J.; Swanson, R. *Electron Devices, IEEE Trans.* **1980**, *27*, 2217–2225.
(18) Gaudin, O.; Jackman, R. B.; Nguyen, T.-P.; Le Rendu, P. *J. Appl. Phys.* **2001**, *90*, 4196.

(19) Lee, C.-W.; Renaud, C.; Hsu, C.-S.; Nguyen, T.-P. *Nanotechnology* **2008**, *19*, 455202.
(20) Tang, J.; Wang, X.; Brzozowski, L.; Barkhouse, D. A. R.; Debnath, R.; Levina, L.; Sargent, E. H. *Adv. Mater.* **2010**, *22*, 1398−402.
(21) Cuff, K. F.; Ellet, M. R.; Kuglin, C.; Williams, L. *7th Int. Conf. Phys. Semicond.* **1964**, 677.
(22) Clifford, J. P.; Johnston, K. W.; Levina, L.; Sargent, E. H. *Appl. Phys. Lett.* **2007**, *91*, 253117.
(23) Hyun, B.-r.; Zhong, Y.-w.; Bartnik, A. C.; Sun, L.; Abruña, H. D.; Wise, F. W.; Goodreau, J. D.; Matthews, J. R.; Leslie, T. M.; Borrelli, N. F. *ACS Nano* **2008**, *2*, 2206−12.
(24) Pattantyus-Abraham, A. G.; Kramer, I. J.; Barkhouse, A. R.; Wang, X.; Konstantatos, G.; Debnath, R.; Levina, L.; Raabe, I.; Nazeeruddin, M. K.; Grätzel, M.; Sargent, E. H. *ACS Nano* **2010**, *4*, 3374−80.
(25) Voznyy, O.; Zhitomirsky, D.; Stadler, P.; Ning, Z.; Hoogland, S.; Sargent, E. H. *ACS Nano* **2012**, *6*, 8448−55.
(26) Konstantatos, G.; Sargent, E. H. *Appl. Phys. Lett.* **2007**, *91*, 173505.
(27) Taylor, D.; Gomes, H. *Conference on Electrical Insulation and Dielectric Phenomena*; IEEE, Piscatway, NJ, 1995; pp 642−645.